ESC European Society of Cardiology

Cardiovascular Research (2023) **119**, 2522–2535
https://doi.org/10.1093/cvr/cvad155

Targeted activation of human ether-à-go-go-related gene channels rescues electrical instability induced by the R56Q$^{+/-}$ long QT syndrome variant

Ravichandra Venkateshappa [1], Diana V. Hunter [1], Priya Muralidharan [1], Raghu S. Nagalingam[1,2], Galvin Huen[1], Shoaib Faizi[1], Shreya Luthra [1], Eric Lin[1], Yen May Cheng[1], Julia Hughes[1], Rania Khelifi[1], Daman Parduman Dhunna[1], Raj Johal[1], Valentine Sergeev[1], Sanam Shafaattalab[1], Lisa M. Julian[3], Damon T. Poburko[1], Zachary Laksman [4], Glen F. Tibbits[1,2,5], and Tom W. Claydon [1]*

[1]Department of Biomedical Physiology and Kinesiology, Simon Fraser University, 8888 University Drive, Burnaby, BC, CanadaV5A 1S6; [2]Cellular and Regenerative Medicine Centre, British Columbia Children's Hospital Research Institute, 938 W 28th Ave, Vancouver, BC, Canada V5Z 4H4; [3]Department of Biological Sciences, Simon Fraser University, 8888 University Drive, Burnaby, BC, CanadaV5A 1S6; [4]Department of Medicine, School of Biomedical Engineering, University of British Columbia, 2194 Health Sciences Mall, Vancouver, BC, Canada V6T 1Z3; and [5]Department of Molecular Biology and Biochemistry, Simon Fraser University, 8888 University Drive, Burnaby, BC, CanadaV5A 1S6

Received 9 November 2022; revised 22 June 2023; accepted 10 July 2023; online publish-ahead-of-print 21 September 2023

Time of primary review: 56 days

Aims

Long QT syndrome type 2 (LQTS2) is associated with inherited variants in the cardiac human ether-à-go-go-related gene (hERG) K^+ channel. However, the pathogenicity of hERG channel gene variants is often uncertain. Using CRISPR–Cas9 gene-edited hiPSC-derived cardiomyocytes (hiPSC-CMs), we investigated the pathogenic mechanism underlying the LQTS-associated hERG R56Q variant and its phenotypic rescue by using the Type 1 hERG activator, RPR260243.

Methods and results

The above approaches enable characterization of the unclear causative mechanism of arrhythmia in the R56Q variant (an N-terminal PAS domain mutation that primarily accelerates channel deactivation) and translational investigation of the potential for targeted pharmacologic manipulation of hERG deactivation. Using perforated patch clamp electrophysiology of single hiPSC-CMs, programmed electrical stimulation showed that the hERG R56Q variant does not significantly alter the mean action potential duration (APD_{90}). However, the R56Q variant increases the beat-to-beat variability in APD_{90} during pacing at constant cycle lengths, enhances the variance of APD_{90} during rate transitions, and increases the incidence of 2:1 block. During paired S1–S2 stimulations measuring electrical restitution properties, the R56Q variant was also found to increase the variability in rise time and duration of the response to premature stimulations. Application of the hERG channel activator, RPR260243, reduces the APD variance in hERG R56Q hiPSC-CMs, reduces the variability in responses to premature stimulations, and increases the post-repolarization refractoriness.

Conclusion

Based on our findings, we propose that the hERG R56Q variant leads to heterogeneous APD dynamics, which could result in spatial dispersion of repolarization and increased risk for re-entry without significantly affecting the average APD_{90}. Furthermore, our data highlight the antiarrhythmic potential of targeted slowing of hERG deactivation gating, which we demonstrate increases protection against premature action potentials and reduces electrical heterogeneity in hiPSC-CMs.

Keywords

hERG • Kv11.1 • hiPSC-CM • hERG activators • RPR260243 • Electrophysiology • Long QT syndrome (LQTS) • Cardiac arrhythmia

* Corresponding author. Tel: +1 778 782 8514; fax: +1 778 782 3040, E-mail: thomas_claydon@sfu.ca

1. Introduction

Human ether-à-go-go-related gene (hERG) voltage-gated K^+ channels are critical for repolarization of the cardiac membrane potential.[1] Inherited genetic variants in *KCNH2*, the gene that encodes hERG channels, often cause channel dysfunction that reduces hERG currents.[1] Loss of hERG channel function delays repolarization and prolongs the action potential duration (APD), which increases vulnerability to early afterdepolarizations, which can result in triggered activity and arrhythmia.[2] Such APD prolongation underlies long QT syndrome (LQTS) and predisposes individuals to a lethal ventricular arrhythmia; torsades de pointes.[3] LQTS Type 2 (LQTS2) is caused by genetic variants in hERG channels and accounts for ~35% of all LQTS cases.[4]

Despite the development of genotype-guided risk stratification profiles and therapeutic strategies,[5] evaluating an individual's risk of a cardiac event can be challenging.[6] In addition, ~25% of individuals that are genotype positive for an LQTS-causing variant have a normal QT interval,[7] and the precipitating factor(s) that may trigger a cardiac event can be elusive.[8] An encouraging opportunity to address these issues has recently been realized through the generation and analysis of patient-derived and isogenic human-induced pluripotent stem-cell-derived cardiomyocytes (hiPSC-CMs).[9] This system facilitates electrophysiological scrutiny of the electrical consequences of specific channel variants and the opportunity for the identification of targeted pharmacological correction.[9,10]

Several studies have highlighted the promise of using hERG variant-carrying hiPSC-CMs to investigate treatment with hERG-specific small molecule activators.[9,10] However, Type 2 hERG activators, which primarily reduce channel inactivation, are associated with an overcorrection of hERG function and predisposition to early repolarization-induced arrhythmia.[10,11] Similarly, using a trafficking chaperone, lumacaftor, which may facilitate hERG channel expression, produced an apparent variant-sensitive exacerbation of the phenotype and/or lack of translation of the improved phenotype back to the patient.[12] While these approaches have been associated with a potential risk for proarrhythmia, Type 1 hERG activators, such as RPR260243, which primarily slow down channel deactivation, may provide safer targeted antiarrhythmic actions.[13,14] Our previous HEK cell and *in silico* studies using the hERG R56Q LQTS-associated variant showed that RPR260243 rescued lost hERG protective currents in response to premature depolarizations, producing a targeted increase in hERG repolarizing drive in the early refractory period without APD shortening.[14] In the present study, we explore the targeted antiarrhythmic potential of the Type 1 hERG activator RPR260243 in hiPSC-CMs by investigating three aims: (i) utilizing CRISPR–Cas9 technology to engineer the hERG R56Q$^{+/-}$ variant in isogenic hiPSC-CMs; (ii) characterizing the effects of the hERG R56Q$^{+/-}$ variant on the markers of arrhythmogenicity; and (iii) exploring the antiarrhythmic potential of the classical Type 1 hERG activator, RPR260243.

2. Methods

2.1 Generation of CRISPR–Cas9 gene-edited cell lines

CRISPR–Cas9 editing of WiCell iPS(IMR90)-1 hiPSCs was performed by transfecting cultured cells at a density of 100 000–200 000 cells per well of a 24-well plate with R56Q sgRNA, Cas9, and GFP cloned into a modified pCCC vector (see Supplementary Material for detailed methods). A 127 bp ssODN complementary to the sense strand, with 38 bases (PAM-distal) and 89 bases (PAM-proximal) on either side of the expected double-stranded break site, was used to provide the template for homology-directed repair and included the hERG c.167G > A (p.Arg56Gln) mutation, as well as a silent mutation (c.174G > A) in the PAM site. Following Accutase (STEMCELL Technologies, 07920; Burnaby, Canada) dissociation, GFP-positive cells were selected by FACS (Becton Dickinson FACSAria Fusion Cell Sorter; East Rutherford, New Jersey), seeded onto Matrigel® (Corning, Glendale, Arizona, CLS356234) and cultured in mTeSR™ Plus (STEMCELL Technologies, 100-0276) supplemented with penicillin–streptomycin (Life Technologies, Carlsbad, California, 15140122) and CloneR™ (STEMCELL Technologies, 05888). After 7–10 days in culture, individual colonies were transferred into a 96-well plate for further growth and analysis. Once confluent, a sample from each individual clone was lysed using DirectPCR lysis reagent with proteinase K solution (Viagen, Los Angeles, California, 301-C and 501-PK), and the lysate was used as the polymerase chain reaction (PCR) template to amplify the region around the hERG R56 site for Sanger sequencing genotyping (GENEWIZ, Azenta Life Sciences, South Plainfield, New Jersey). Selected clones were expanded and cryopreserved using mFreSR™ (STEMCELL Technologies, 05855). Top-ranked potential off-target sites predicted using CRISPOR (http://crispor.tefor.net/)[15] were also sequenced, and no off-target mutations were identified.

2.2 Directed differentiation of hiPSCs to cardiomyocytes

Differentiation of hiPSC clones was performed following the standardized STEMdiff™ Ventricular Cardiomyocyte Differentiation Kit protocol (STEMCELL Technologies, 05010), as per the manufacturer's guidelines. Briefly, hiPSC clones were seeded as small aggregates onto Matrigel® and cultured with mTeSR™ Plus and the ROCK inhibitor 10 μM Y-27632 (Biogems, West Lake Village, California, 1293823) prior to timed media changes as per the kit protocol. Beating monolayers could be identified ~7–10 days after the start of differentiation and were dissociated following procedures in the STEMdiff™ Cardiomyocyte Dissociation Kit (STEMCELL Technologies, 05025). Briefly, following washing in Dulbecco's Phosphate Buffered Saline (D-PBS, VWRL0119-0500, Radnor, Pennsylvania), the cells were treated with STEMdiff™ Cardiomyocyte Dissociation Medium for 7–10 min and then resuspended in STEMdiff™ Cardiomyocyte Support Medium onto 12 mm glass coverslips (VWR, 89015-725) coated with 10 μg/mL fibronectin (Gibco, Waltham, Massachusetts, PHE0023). Electrophysiological and immunocytochemical analyses of the cells were performed 4–10 days after replating. Data were obtained from cells derived from several differentiations (5 in the case of wild-type (WT) sham, and 4 in the case of hERG R56Q).

2.3 Cellular phenotyping of hiPSC-CM clones

Cardiomyocyte markers were evaluated using immunocytochemistry (see Supplementary Material for detailed methodology). Briefly, following permeabilization, the cells were probed overnight at 4°C with mouse monoclonal anticardiac troponin T (cTnT; 1:1000; Invitrogen, Waltham, Massachusetts, MA5-12960) and rabbit monoclonal anti-α-actinin (Invitrogen, 710947), followed the next day by 2 h incubation at room temperature with the secondary antibodies, Alexa Fluor 488-conjugated goat antimouse (1:1000; Invitrogen, A-11029) and Alexa Fluor 555-conjugated goat antirabbit (1:1000; Invitrogen, A32732). Cell nuclei were counterstained with Hoechst 33342 (Abcam, Cambridge, UK, ab228551). Following fixation, the cells were mounted using ProLong Glass Antifade Mountant (Thermo Scientific, Waltham, Massachusetts, P36980), and images were acquired on a Nikon Ti-E inverted epifluorescence microscope. Reverse transcriptase–PCR (RT–PCR) was used to evaluate qualitative transcript levels of pluripotency and cardiomyocyte markers in undifferentiated hiPSCs and differentiated hiPSC-CMs (see Supplementary Material). Western blot was used to determine the relative expression of hERG1a and hERG1b proteins from the monolayers of hiPSC-CMs from different methods of differentiation. Divergence in N-terminal protein sequence enabled isoform-specific immunolabelling of hERG1a (Cell Signaling Technology, Danvers, Masschusetts, D1Y2J, rabbit monoclonal, 1:1000) and hERG1b (Enzo Life Sciences, Farmingdale, New York, ALX-215-51, rabbit polyclonal, 1:1000).

2.4 Electrophysiology

Electrophysiological recordings were performed as outlined in Supplementary Material. Briefly, signals were acquired at 37°C from single-

beating cardiomyocytes using an Axon Instruments 200B amplifier (Molecular Devices, San Jose, California) and perforated patch clamp. Borosilicate glass electrodes with a tip resistance of 2.5–3 MΩ were filled with an internal solution supplemented with 140–170 μg/mL amphotericin B. The rapidly activating potassium current (I_{Kr}) was recorded during 2 s voltage clamp steps from −60 to +40 mV in 20 mV increments (holding potential was −40 mV), followed by a 3 s step to −40 mV to monitor deactivation. Ten micromolar of nifedipine was used to stop beating, and I_{Kr} was measured in the absence and presence of 10 μM dofetilide. The dofetilide-sensitive I_{Kr} current was used for analysis.

Selected cells for action potential recordings demonstrated a negative diastolic membrane potential and a long plateau phase as characteristic features of ventricular-like action potentials. Cells that failed to exhibit a prominent plateau phase and more negative membrane potential were excluded from the experiment. To further validate the selection of ventricular-like cells, the APD_{90}–APD_{50}/APD_{90} ratio, the repolarization fraction, was measured.[16] The mean repolarization fraction of the cells used in this study was 0.29 ± 0.01, which is indicative of ventricular-like cells.[17] To record action potentials, 2 ms current pulses were applied at 1.5–2×, the stimulation threshold. S1–S2 paired stimulations were applied at coupling intervals ranging from 110 to 500 ms following a train of eight S1 stimuli. A dynamic stimulation procedure involved stimulating cells for 30 beats at progressively shorter basic cycle lengths (BCLs) from 500 to 167 ms.

2.5 Data analysis and statistics

Exponential fits of I_{Kr} deactivation and action potential peak detection and parameter measurement [maximum diastolic potential (MDP), action potential amplitude, APD_{30}, APD_{90}, and rise time] were conducted using Clampfit software (Axon Instruments). The diastolic interval (DI) was measured as the difference in time interval between the stimulus and the APD_{90} of the preceding action potential. The effective refractory period (ERP) was measured as the longest cycle length that failed to capture a ventricular response. We defined the loss of ventricular response as a depolarization with a rise time of >2 ms and a decay time of 30% from the peak of >40 ms. The post-refractory repolarization period (PRRP) was measured as the difference between the ERP and the APD_{90} of the preceding action potential.

All data are expressed as mean ± SEM (n = sample size). Data were tested for normality (Shapiro–Wilk) and data sets that failed normality were log-transformed prior to statistical testing. The box plots represent the first quartile, median, and third quartile. Whiskers represent minimum and maximum values, and the dashed line indicates the mean. Statistical comparisons between means were conducted using one-way or two-way analysis of variance (ANOVA) with a Holm–Sidak *post hoc* test and repeated measures as appropriate, with $P < 0.05$ used as an indicator for statistical significance. Sample variance, σ, was calculated as the SD2, and significant differences in sample variance were determined using a two-tailed F-test with $P < 0.05$ as an indicator of a difference. Regression analyses were performed using Pearson correlations for normally distributed data and Spearman correlations for non-parametric tests.

3. Results

3.1 hiPSC-CMs harbouring the CRISPR-edited hERG R56Q$^{+/-}$ variant display rapidly deactivating I_{Kr} that is slowed by the hERG activator, RPR260243

We used CRISPR–Cas9-induced homology-directed repair mechanisms in cultured hiPSCs to engineer a precise a.167G > A heterozygous edit in the hERG gene that generated the LQTS2-associated hERG p.Arg56Gln (R56Q$^{+/-}$) PAS domain variant (*Figure 1A* and *B*). hiPSC clones were differentiated into beating hiPSC-CM monolayers that stained for cTnT and alpha-actinin (ACTN2) in both monolayer format (see Supplementary material online, *Figure S1*) and when plated as individual cells (*Figure 1C*). RT–PCR measures (see Supplementary material online, *Figure S1*) further demonstrated successful transcript reprogramming. The use of WT sham hiPSCs, i.e. un-edited hiPSCs following CRISPR, provided a stringent isogenic control that reduces the confounding effects of putative off-target Cas9 edits. Introduction of the hERG R56Q$^{+/-}$ edit did not affect the relative membrane expression ratio of hERG1a and hERG1b protein (*Figure 1D*).

Figure 1E–G shows representative recordings of dofetilide-sensitive I_{Kr} from WT sham and hERG R56Q hiPSC-CMs during voltage clamp of single cells. Consistent with the well-described phenotypic gating disturbance of the LQTS-associated hERG R56Q variant,[18] deactivation kinetics were accelerated in hERG R56Q cells: the τ of deactivation was reduced from 1.43 ± 0.2 s in WT sham cells ($n = 3$) to 0.33 ± 0.05 s in hERG R56Q cells ($n = 5$; $P = 0.008$, one-way ANOVA with Holm–Sidak *post hoc* test; *Figure 1H*). Since one aim of this study was to investigate the antiarrhythmic potential of targeting hERG channels with the selective activator, RPR260243, we also measured its effect on I_{Kr} in these cells. *Figure 1G* and *H* shows that the application of 10 μM RPR260243 slowed deactivation in hERG R56Q hiPSC-CMs: the τ of deactivation at –40 mV was increased to 1.30 ± 0.26 s ($n = 5$; $P = 0.011$ when compared with R56Q cells without RPR260243, one-way ANOVA, with Holm–Sidak *post hoc* test). These data demonstrate that I_{Kr} deactivation is accelerated in hERG R56Q hiPSC-CMs and that the hERG channel activator, RPR260243, slows deactivation of I_{Kr} in hiPSC-CMs.

3.2 Effect of the hERG R56Q variant and RPR260243 on action potential characteristics in hiPSC-CMs

To explore the phenotypic consequences of the R56Q variant and RPR260243, we recorded action potential characteristics in single-beating WT sham and hERG R56Q hiPSC-CMs in the absence and presence of 10 μM RPR260243. Steady-state action potentials recorded during a stimulation train at 2 Hz (500 ms BCL) were ventricular-like in morphology (*Figure 2A*). We observed no differences in the MDP or peak action potential amplitude (*Figure 2B* and *Table 1*) between WT sham and hERG R56Q cells ($P = 0.434$ and 0.965, respectively; two-way ANOVA with Holm–Sidak *post hoc* test). The average APD at 90% repolarization was 253 ± 11 ms in WT sham cells and 278 ± 19 ms in hERG R56Q ($P = 0.288$; two-way ANOVA with Holm–Sidak *post hoc* test). While the mean APD_{90} values were not statistically different, there was marked variability in the APD_{90} in hERG R56Q hiPSC-CMs that was not present in WT sham cells, or in other parameters, i.e. MDP, and amplitude (*Figure 2B*). The variance, σ (SD^2), of the APD_{90} was increased from 1375 ms^2 in WT sham cells to 3805 ms^2 in hERG R56Q cells ($P = 0.051$, F-test). Similarly, while the mean APD_{30} value was not affected by the hERG R56Q variant [APD_{30} values were 139 ± 6 ms in WT sham cells and 139 ± 13 ms in hERG R56Q ($P = 0.974$; two-way ANOVA with Holm–Sidak *post hoc* test)], the variance of APD_{30} was increased from 469 ms^2 in WT sham cells to 1834 ms^2 in hERG R56Q cells ($P = 0.017$, F-test). The mean index of triangulation (APD_{90}–APD_{30}) was not different in hERG R56Q cells compared with that in WT sham cells (*Figure 2B*; $P = 0.084$; two-way ANOVA with Holm–Sidak *post hoc* test). The hERG channel activator, RPR260243, had no significant effects on steady-state action potential characteristics in either WT sham or hERG R56Q hiPSC-CM lines (*Figure 2*, *Table 1*) consistent with previous observations in animal models.[19]

3.3 Effects of the R56Q variant and RPR260243 on the ventricular response to premature stimulations in hiPSC-CMs

Our working hypothesis is that R56Q variant pathogenicity may result from reduced protection against premature depolarizations, rather than effects on steady-state action potential characteristics. To test this, we investigated action potential restitution properties in WT sham and hERG R56Q hiPSC-CMs using a standard S1–S2 stimulation paradigm to determine how the APD_{90} of the response to the S2 stimulation depended on the preceding DI (*Figure 3*). These standard electrical restitution curves

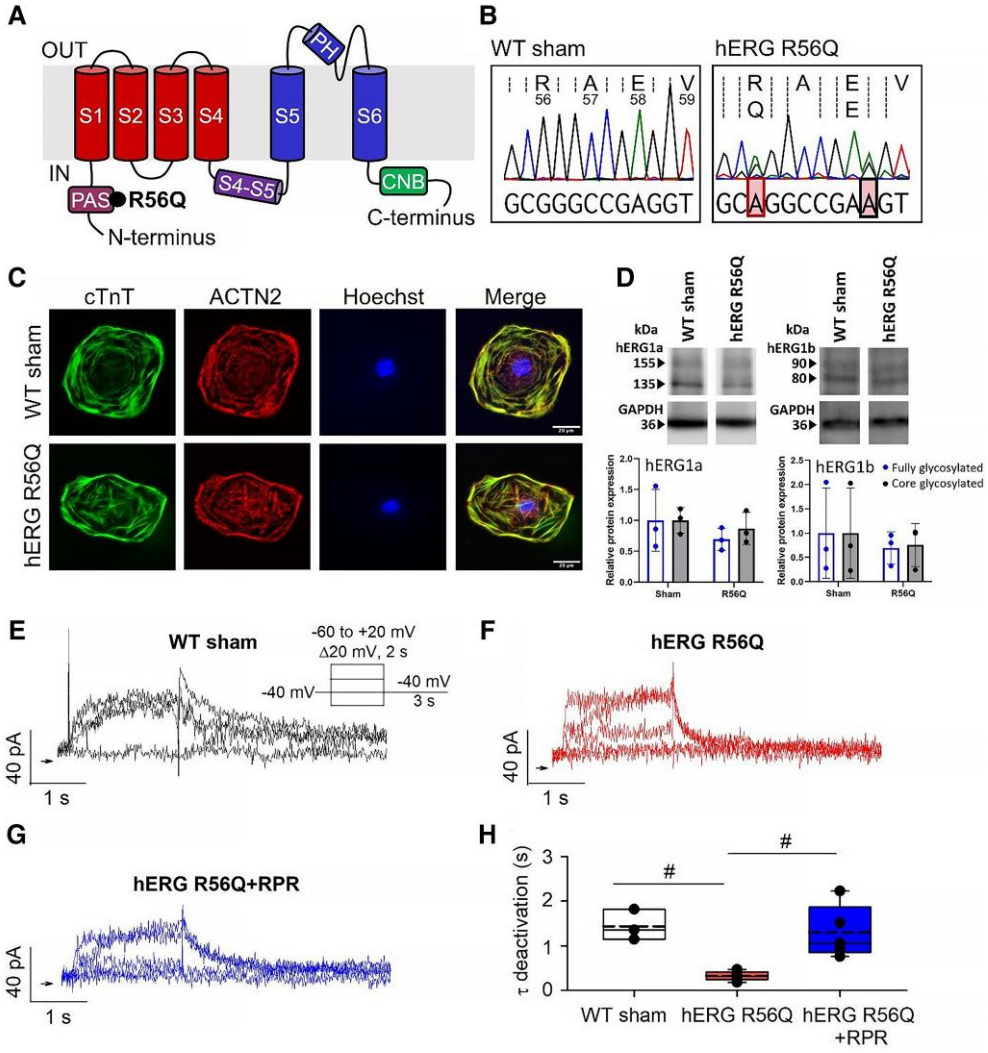

Figure 1 Generation of the hERG R56Q variant in hiPSCs. (*A*) The hERG R56Q variant is located within the PAS domain of the hERG channel. (*B*) Chromatograms from the sequencing of a WT sham clone and a heterozygous hERG R56Q clone with the G to A substitution at both the mutation site causing the R to Q amino acid change and at the PAM site where the substitution creates a silent mutation that disrupts the PAM binding site and prevents further Cas9 binding in edited cells. (*C*) Selected WT sham and hERG R56Q clones were successfully differentiated into beating cardiomyocytes that stained for the cardiac markers cTNT and ACTN2. (*D*) Example western blots showing isoform-specific immunolabelling of hERG1a or hERG1b in WT sham and hERG R56Q hiPSC-CMs. The average ratio of fully glycosylated (mature) and core glycosylated (immature) protein from densitometry measurement of bands from three different cell lysate samples is shown. (*E* and *F*) Representative I_{Kr} traces recorded from WT sham (*E*), hERG R56Q (*F*), and hERG R56Q with 10 μM RP260243 (*G*; hERG R56Q + RPR) during the voltage clamp protocol shown in the inset. (*H*) Box plot of deactivation time constant (τ) at −40 mV. WT sham $n = 3$; hERG R56Q $n = 5$; hERG R56Q + RPR260243 $n = 5$. $^{\#}P \leq 0.05$ (one-way repeated measures ANOVA with Holm–Sidak *post hoc* test).

(ERCs) describe adaptation of cellular action potentials to acute changes in DI. In WT sham cells, the maximum ERC slope was 3.1 ± 0.6 (*Figure 3A*; $n = 7$). To the best of our knowledge, this is the first report of the maximal ERC slope in hiPSC-CMs. The maximum ERC slope in hERG R56Q cells was 3.4 ± 0.5 (*Figure 3B*; $n = 15$), which was not significantly different from that observed in WT sham cells ($P = 0.789$; two-way repeated measures ANOVA with Holm–Sidak *post hoc* test; *Table 2*). In the presence of RPR260243, the maximal slope of the ERC was 2.5 ± 0.3 (*Figure 3C*; $n = 7$) in WT sham cells and 4.0 ± 0.8 (*Figure 3D*; $n = 15$) in hERG R56Q cells ($P = 0.573$ and 0.750, respectively, compared with pre-drug control, two-way repeated measures ANOVA with Holm–Sidak *post hoc* test).

The implications of the ERC slope are debated; however, because a slope of >1 has been associated with the development of alternans and ventricular fibrillation (VF) in humans and other mammals, we measured and compared the minimum DI at which the ERC slope became >1 in the different cell lines and conditions. In WT sham cells, the ERC slope became >1 at a DI of 48.3 ± 4.5 ms, which was not significantly different from that in hERG R56Q cells (61.4 ± 8.2 ms; $P = 0.263$; *Table 2*). The presence of RPR260243 had no significant effect on the DI at which the slope >1 in either cell line: the DI was 51.6. ± 4.2 ms in WT sham cells and 74.5 ± 6.1 ms in hERG R56Q cells ($P = 0.612$ and 0.099, respectively, compared with pre-drug control, two-way repeated measures ANOVA with Holm–Sidak *post hoc* test).

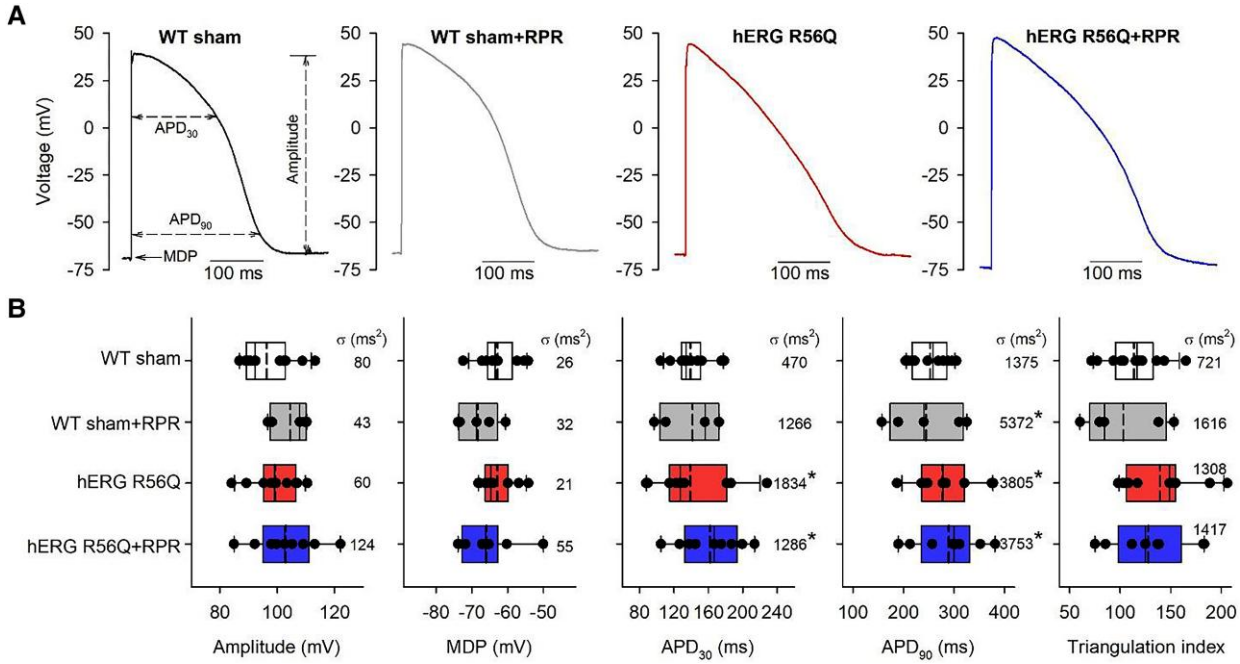

Figure 2 Steady-state action potential properties. (*A*) Representative steady-state action potential recordings at 500 ms BCL from WT sham and hERG R56Q hiPSC-CMs in the absence and presence of 10 μM RPR260243. The final action potential in the train of 20 is shown. (*B*) Box plot representations of steady-state action potential characteristics. MDP, maximum diastolic potential; APD_{30}, action potential duration at 30% of repolarization; APD_{90}, action potential duration at 90% of repolarization; triangulation index, APD_{90}–APD_{30} (see *A*). WT sham $n = 5$; WT sham + RPR $n = 5$; hERG R56Q $n = 9$; hERG R56Q + RPR $n = 9$. Each dot represents the average of 20 steady-state action potentials in one cell. The variance, σ (ms^2), of each parameter is indicated. There were no significant differences in any action potential parameter between different groups (two-way repeated measures ANOVA with Holm–Sidak *post hoc* test). *Significantly different variance between groups ($P \leq 0.05$; *F*-test).

Table 1 Steady-state action potential characteristics in WT sham and hERG R56Q hiPSC-CMs recorded at 2 Hz

	WT sham ($n = 12$)	WT sham + RPR260243 ($n = 5$)	hERG R56Q ($n = 11$)	hERG R56Q + RPR260243 ($n = 9$)
Amplitude (mV)	96.3 ± 2.6	104.5 ± 2.9	99.1 ± 2.3	102.9 ± 3.7
MDP (mV)	−62.8 ± 1.5	−68.3 ± 2.5	−62.9 ± 1.4	−66.0 ± 2.5
APD_{30} (ms)	139 ± 6	142 ± 16	139 ± 13	162 ± 12
APD_{90} (ms)	253 ± 11	245 ± 33	278 ± 19	290 ± 20
APD_{90}–APD_{30} (ms)	114 ± 8	103 ± 18	139 ± 11	128 ± 13

No significant differences between parameters were observed.

3.4 The R56Q variant and RPR260243 application affect the membrane response to premature depolarizations

While the maximal steepness of the ERC relationship was not greatly influenced by the R56Q variant or by RPR260243 application, analysis of the membrane voltage responses to paired S1–S2 stimulations enabled quantitative assessment of cellular responses to premature depolarization. We measured the difference between the ERP and the APD_{90} of the action potential initiated by the penultimate S1, which yields the post-repolarization refractory period (PRRP = ERP – APD_{90}) that is a known indicator of arrhythmogenicity.[20,21] In WT sham cells, the PRRP was −19.6 ± 4.3 ms ($n = 6$), indicating that short-coupled S2 stimuli arriving prior to 90% repolarization of the S1 action potential are capable of eliciting action potentials, i.e. encroachment occurs (*Figure 4A* and *B*). We hypothesized that the fast repolarization of I_{Kr} in the hERG R56Q variant would reduce repolarizing drive in the early refractory period and allow earlier capture of S2-initiated action potentials. However, while in some hERG R56Q cells, the PRRP was more negative than in WT sham cells; in others, the PRRP was longer such that the average PRRP in hERG R56Q cells was −8.9 ± 6.8 ms ($n = 15$). As a result, while the mean value was not significantly different from that in WT sham cells ($P = 0.402$, two-way repeated measures ANOVA), the cell-to-cell variability in PRRP in hERG R56Q was significantly greater than in WT sham cells (*Figure 4B*): σ was 110.9 ms^2 in WT sham and 696.9 ms^2 in hERG R56Q cells ($P = 0.026$, *F*-test).

We assessed whether the high variance in the PRRP in hERG R56Q cells was related to the high variance in steady-state action potential characteristics observed in these cells in *Figure 2*. We found that hERG R56Q cells with a more negative PRRP had a prolonged steady-state APD_{90} and increased triangulation index (*Figure 4E* and *F*). Indeed, *Figure 4G*

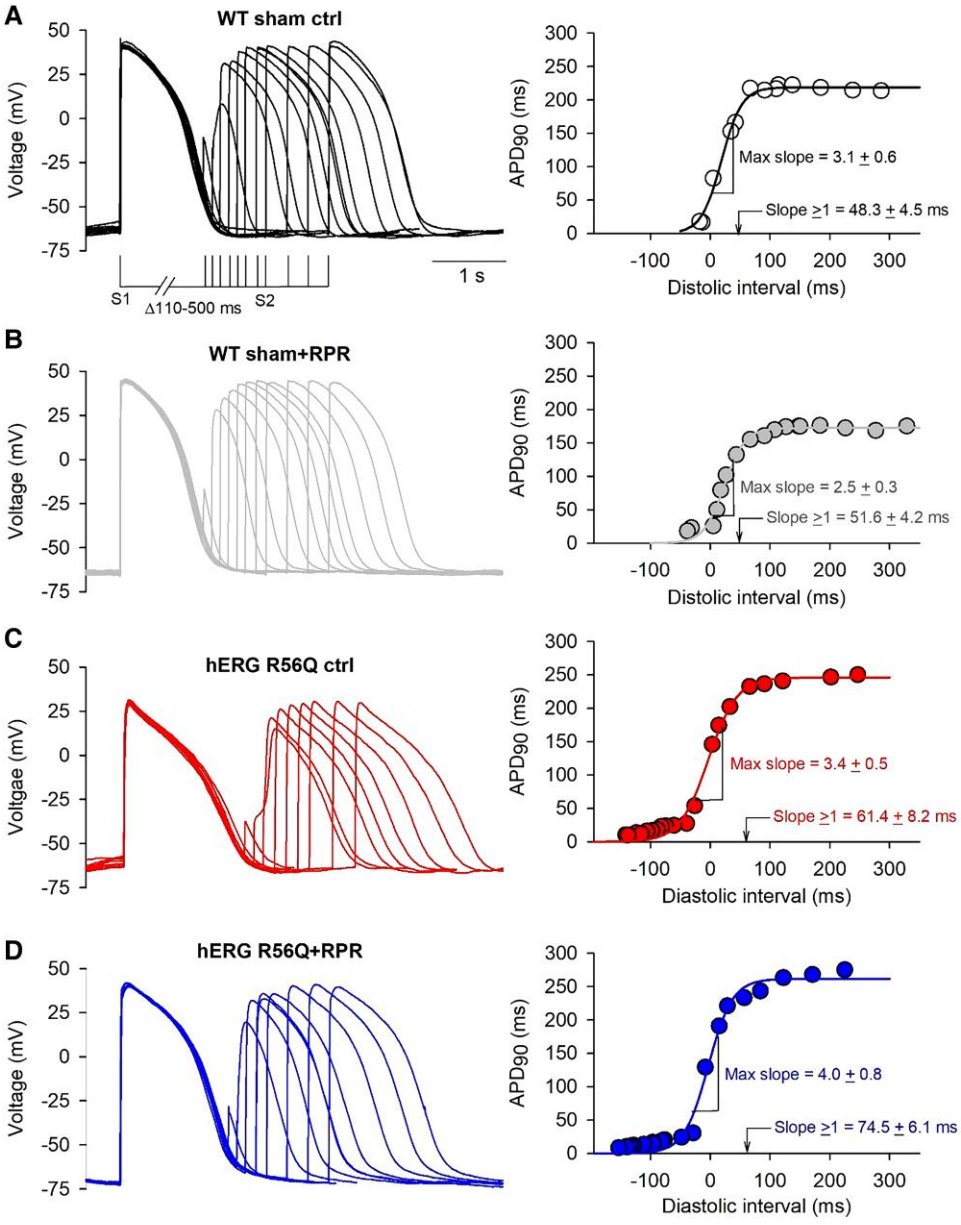

Figure 3 Standard electrical restitution properties of hiPSC-CMs. (*A–D*) Left: Overlay of voltage traces recorded from a representative cell in each condition in response to the current stimulus protocol shown. Membrane responses were recorded during eight S1 stimuli at a BCL of 500 ms followed by a single premature stimulus (S2) at progressively shorter S1–S2 intervals ranging from 500 down to 110 ms. Some captured responses at longer S1–S2 intervals have been removed for clarity. Right: Representative standard APD_{90} restitution curves from an example hiPSC-CM cell in each case. The data were fitted with a sigmoidal function (solid line) and symbols indicate measured APD_{90} at each DI. Mean maximum slope and minimum DI at which the slope became >1 from all 7 WT sham cells and 15 hERG R56Q cells are indicated.

demonstrates a significant correlation between the PRRP in R56Q hERG cells and both the APD_{90} ($R = 78$, $P = 0.001$) and the triangulation index ($R = 0.72$, $P = 0.003$). There was also a correlation in these cells between the PRRP and the ERP/APD_{90} ratio ($R = 0.97$, $P < 0.0001$), where cells with a more negative PRRP had a low ERP/APD_{90} ratio indicative of susceptibility to premature ventricular activity and arrhythmogenicity in cells showing encroachment.[20,22] There was no correlation between the PRRP and the MDP in R56Q hERG cells ($R = 0.33$, $P = 0.3844$). These findings suggest the presence of heterogeneity in the balance of repolarization and refractoriness in hERG R56Q cells that was not present in WT sham cells. Application of RPR260243 increased the PRRP in both WT sham and hERG R56Q cells (*Figure 4C* and *D*). This effect was observed regardless of the heterogeneity in hERG R56Q behaviour. The presence of 10 μM RPR260243 increased the PRRP by 13.1 ± 4.8 and 26.8 ± 7.7 ms in WT sham ($P = 0.040$) and hERG R56Q ($P \leq 0.001$) cells, respectively. In hERG R56Q variant cells with a negative PRRP, RPR260243 not only reduced the encroachment, but also decreased both the APD_{90} and the triangulation index (*Figure 4E* and *F*, *Table 3*).

The characteristics of the earliest captured ventricular response (ECVR) to short-coupled S1–S2 stimulation pairs in hERG R56Q cells also displayed substantial heterogeneity compared with WT sham cells

Table 2 ERC properties

	WT sham ($n = 7$)	WT sham + RPR260243 ($n = 7$)	hERG R56Q ($n = 15$)	hERG R56Q + RPR260243 ($n = 15$)
Standard ERC				
Max slope	3.1 ± 0.6	2.5 ± 0.3	3.4 ± 0.5	4.0 ± 0.8
DI at slope >1 (ms)	48.3 ± 4.5	51.6 ± 4.2	61.4 ± 8.2	74.5 ± 6.1
Dynamic ERC				
Max slope	2.0 ± 0.3	1.7 ± 0.2	2.1 ± 1.1	2.3 ± 0.4
DI at slope >1 (ms)	57.8 ± 6.6	70.7 ± 4.3	70.2 ± 6.0	81.9 ± 7.3

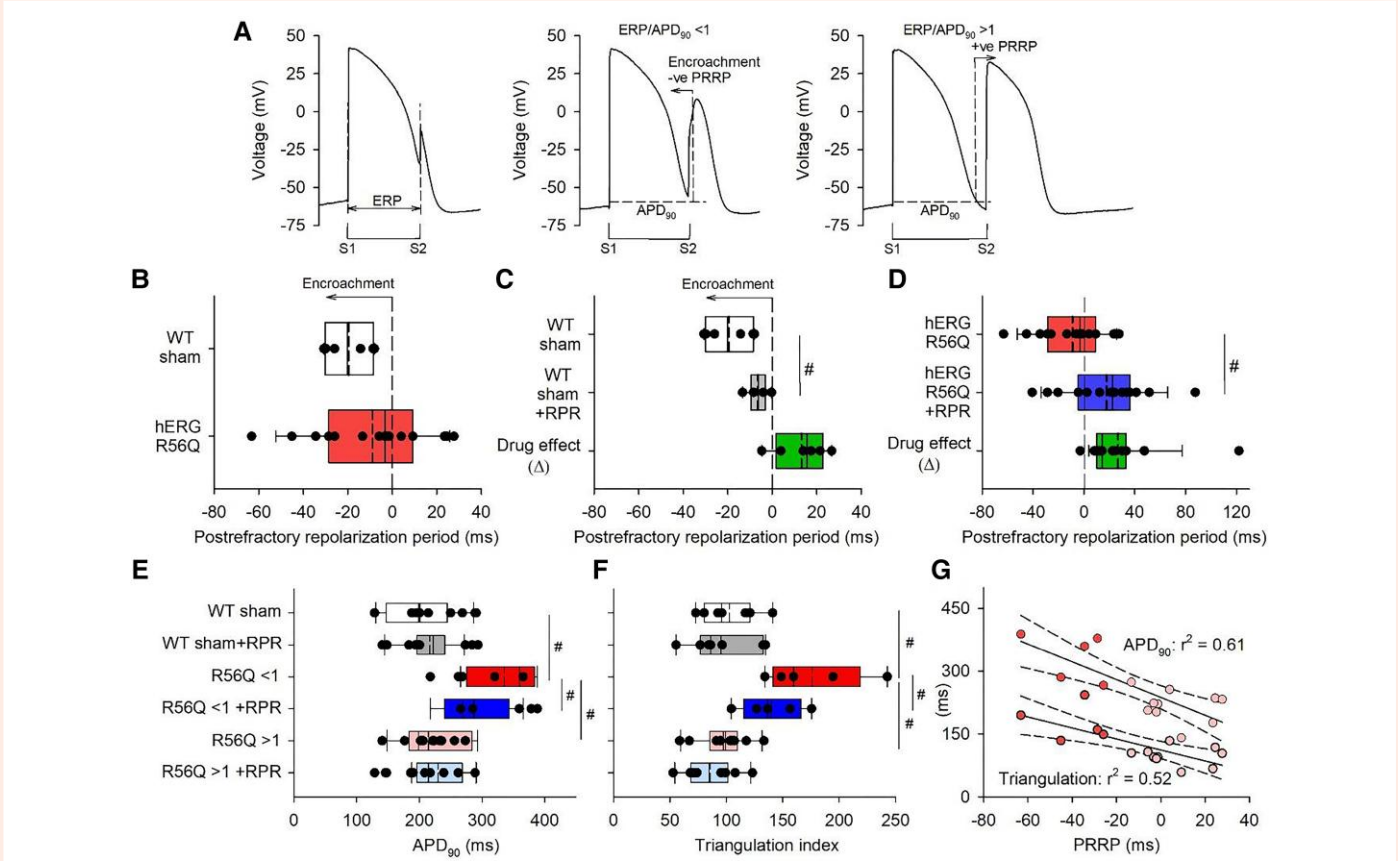

Figure 4 PRRP and the ERP/APD_{90} ratio. (*A*) Annotated descriptions of the ERP, PRRP, and ERP/APD_{90} ratio. Note that a negative PRRP reflects encroachment and an ERP/APD_{90} ratio <1, while a positive PRRP reflects that the APD_{90} is shorter than the ERP (ERP/APD_{90} ratio >1). (*B–D*) Box plot representations showing the effect of the hERG R56Q variant and 10 μM RPR260243 on the PRRP. (*B*) Comparison of WT sham ($n = 7$) with hERG R56Q ($n = 15$). (*C*) Comparison of the PRRP in WT sham cells ($n = 7$) with and without RPR260243 ($n = 7$). Drug effect (Δ) indicates the difference. (*D*) Comparison of the PRRP in hERG R56Q variant cells with ($n = 15$) and without RPR260243 ($n = 15$). (*E* and *F*) Comparison of steady-state APD_{90} (*E*) and triangulation index (*F*) in WT sham, hERG R56Q ERP/APD_{90} < 1, and hERG R56Q ERP/APD_{90} > 1 cells in the absence and presence of RPR260243. (*G*) Linear regression plots describing the relationship between PRRP and APD_{90} or triangulation index across all hERG R56Q variant cells. Solid lines represent regression fits [r^2 values were 0.61 ($P = 0.001$) and 0.52 ($P = 0.003$) for APD_{90} and triangulation index, respectively] and dashed lines reflect 95% confidence intervals. In all box plots, each dot represents data from a single cell. #Significantly different mean value (two-way repeated measures ANOVA with Holm–Sidak *post hoc* test; $P \leq 0.05$).

(*Figure 5*). The average rise time of the ECVR in WT sham cells was 23.7 ± 1.4 ms with a variance of 11.9 ms^2 ($n = 7$), while the rise time was 37.1 ± 6.3 ms in hERG R56Q cells ($P = 0.276$; compared with WT sham, two-way repeated measures ANOVA) with a σ of 600.0 ms^2 ($P = 0.0002$, *F*-test; $n = 15$). The average APD_{90} of the earliest captured response also tended to be prolonged by the R56Q variant: the average APD_{90} of the earliest captured response was 106 ± 15 ms in WT sham compared with 163 ± 17 ms in hERG R56Q cells ($P = 0.045$; two-way repeated measures ANOVA). Other properties, such as MDP and amplitude, were not significantly different between the WT sham and

Table 3 Biomarkers of arrhythmogenicity in hERG R56Q cells

	WT sham	WT sham + RPR	hERG R56Q ERP/APD_{90} < 1	hERG R56Q ERP/APD_{90} < 1 + RPR	hERG R56Q ERP/APD_{90} > 1	hERG R56Q ERP/APD_{90} > 1 + RPR
PRRP (ms)	−19.6 ± 4.3	−6.4 ± 1.9[a]	−39.4 ± 6.8	+0.1 ± 23.0[a]	+6.3 ± 4.5[b]	+26.8 ± 4.9[a]
APD_{90} (ms)	229.7 ± 15.1	214.5 ± 20.3	335.4 ± 25.1[c]	286.9 ± 25.6[a]	216.7 ± 12.1[b]	201.4 ± 16.5
Triangulation (ms)	103.0 ± 9.2	95.2 ± 11.0	176.0 ± 19.4[c]	140.0 ± 12.2[a]	97.3 ± 7.0[b]	85.6 ± 6.9

[a]Significantly different from untreated control.
[b]Significantly different from hERG R56Q ERP/APD_{90} < 1.
[c]Significantly different from WT sham.

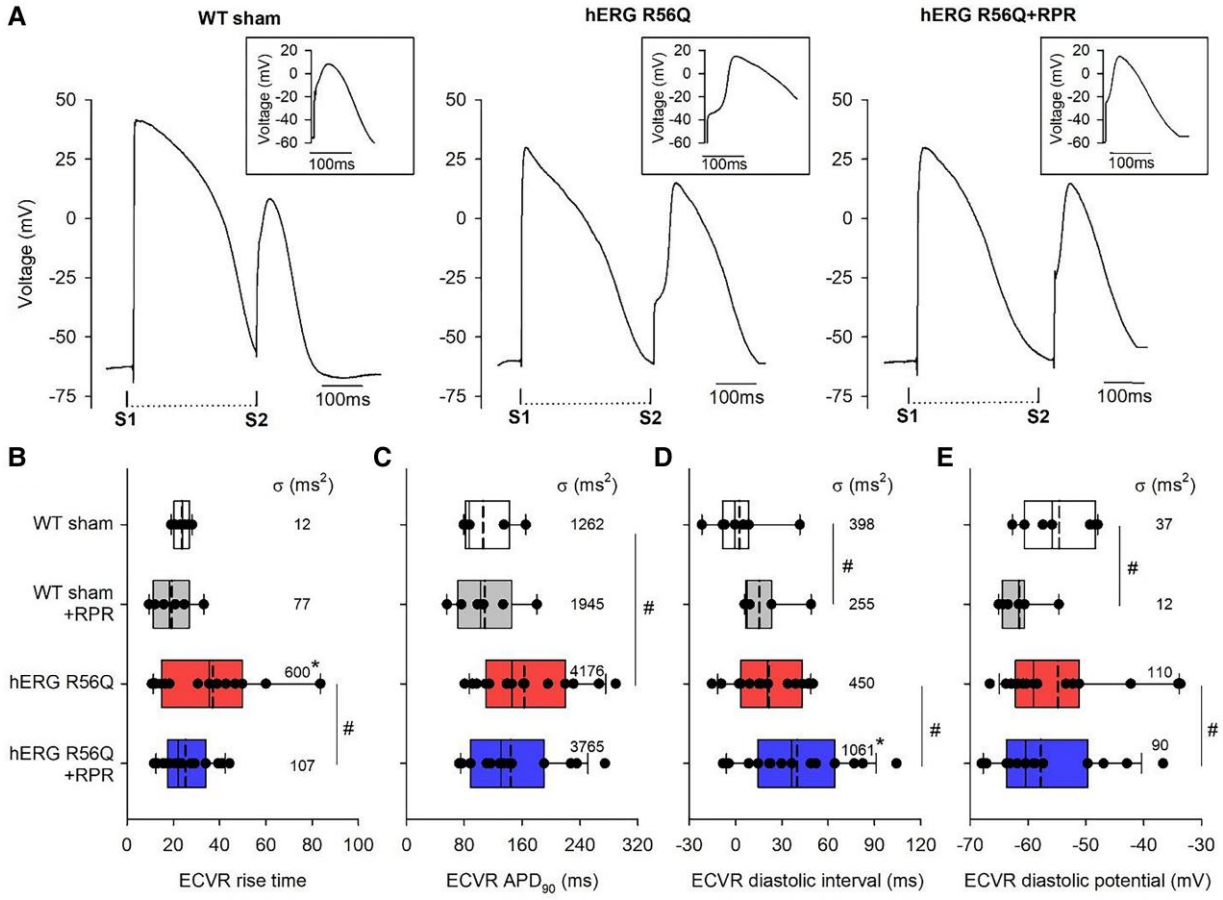

Figure 5 The ECVRs during close-coupled S1–S2 stimulation. (*A*) Representative examples of ECVRs in WT sham, hERG R56Q, and hERG R56Q with 10 μM RPR260243 (hERG R56Q + RPR) during close-coupled S1–S2 stimulations. Insets show the response to the S2 stimulation on a faster time base to highlight the rise time. (*B–E*) Box plot representations of ECVR properties. WT sham $n = 7$; WT sham + RPR $n = 7$; hERG R56Q $n = 15$; hERG R56Q + RPR $n = 15$. Each dot represents data from a single cell and the variance of each group is given. #Significantly different mean value (two-way repeated measures ANOVA with Holm–Sidak *post hoc* test; $P \leq 0.05$). *Significantly different sample variance ($P \leq 0.05$, *F*-test).

hERG R56Q lines. Moreover, application of RPR260243 to hERG R56Q cells reduced the variability of the ECVR (*Figure 5B*). In the presence of 10 μM RPR260243, the rise time of the earliest response in hERG R56Q cells was significantly reduced to 25.3 ± 2.7 ms ($n = 15$; $P = 0.014$ when compared with hERG R56Q in the absence of RPR260243, two-way repeated measures ANOVA), and the variance, σ, was reduced to 106.7 ms^2 ($P = 0.001$, *F*-test). RPR260243 also significantly increased the DI of the ECVR and decreased the diastolic potential reached between S1 and S2 stimuli in both WT sham and hERG R56Q cells (*Figure 5D* and *E*), suggesting that the hERG activator reduced excitability. These observations suggest that the hERG R56Q variant increased heterogeneity in the response to premature stimulations and that RPR260243 reduced this variability and protected against the formation of premature action potentials.

3.5 Effects of the hERG R56Q variant and RPR260243 on action potential adaptation to dynamic rate changes in hiPSC-CMs

The data so far describe the impact of the R56Q variant and RPR260243 application on steady-state action potentials and membrane responses to premature depolarizations. We next investigated action potential responses during dynamic adaptation to progressively shortened BCLs. Initial measurements of the slope of the relationship between APD_{90} and DI during rate changes (dynamic ERC) showed no effect of the hERG R56Q variant, or the application of RPR260243 (*Table 2*). However, consistent with altered refractoriness in the hERG R56Q variant, we observed a greater incidence of loss of capture at shorter BCLs than in WT sham cells. In both WT sham and hERG R56Q cells, 1:1 capture of action potentials occurred at longer BCLs, but as the BCL, shortened 2:1 capture was observed, presumably because the BCL became shorter than the absolute refractory period. The loss of 1:1 capture occurred sooner in hERG R56Q cells than in WT sham cells (see Supplementary material online, *Figure S2*). For example, 1:1 capture was lost in 60% of hERG R56Q cells at a BCL of 333 ms, while 100% of WT sham cells maintained 1:1 capture at this BCL.

We also observed significant differences in how APD_{90} responded to transitions in cycle length in WT sham and hERG R56Q cells (*Figure 6*). Example diary plots of APD_{90} recorded from a WT sham cell in the absence and presence of 10 μM RPR260243 (*Figure 6A*) highlight low APD_{90} variance during BCL transitions (*Figure 6D*). In hERG R56Q cells, we observed more heterogeneous unstable responses to rate changes. hERG R65Q cells with a high PRRP and ERP/APD_{90} ratio showed low variance, but hERG R56Q cells with a negative PRRP and low ERP/APD_{90} ratio showed a high APD_{90} variance with BCL transitions (*Figure 6B–D*). This heterogeneous response to abrupt rate change was reduced by the application of RPR260243, which stabilized rate transitions, decreasing the dispersion of APD_{90} in hERG R56Q cells (*Figure 6B*). For example, the percentage of hERG R56Q cells in 2:1 capture at 333 ms BCL was increased from 40% in control to 60% with 10 μM RPR260243.

In addition to greater instability during rate transitions, we also observed increased beat-to-beat variability in the APD_{90} during constant cycle length pacing in hERG R56Q cells with a negative PRRP and low ERP/APD_{90} ratio. This is represented by Poincaré plots and SD1 analyses in *Figure 7*. The beat-to-beat variability of APD_{90} in WT sham cells was relatively low, but as expected, it slightly increased at the shorter BCL of 250 ms as alternans and 2:1 capture was observed in some cells at this high stimulation rate. The effect of RPR260243 was minor, but it is noteworthy that the hERG activator reduces alternans and stabilizes action potential responses in 2:1 capture at shorter cycle lengths in cells showing less stable APD_{90} beat-to-beat variability (see BCL 250 ms, *Figure 7A*). While the beat-to-beat variability in hERG R56Q cells with a higher PRRP and ERP/APD_{90} ratio was low, the SD1 values describing beat-to-beat variability were significantly higher in hERG R56Q cells with a negative PRRP and low ERP/APD_{90} ratio at each BCL (*Figure 7C–F*, *Table 4*). In hERG R56Q cells with a low ERP/APD_{90} ratio, we observed unstable, variable (dispersed) beat-to-beat APD_{90} values, particularly as the cycle lengths shortened, e.g. 333 ms BCL. *Figure 7G–I* shows that the beat-to-beat variance in APD_{90} was significantly correlated with the PRRP in R56Q variant cells. In R56Q variant cells, RPR260243 reduced the beat-to-beat variability, favouring stable 2:1 capture of action potential firing in place of ectopic action potentials with erratic, variable, APD_{90} (*Figure 7C* and *D*).

4. Discussion

This study provides novel evidence for mechanisms of pathogenicity in LQTS2 variant carriers where the QTc is borderline or normal, i.e. concealed LQTS, and does so using hiPSC-CMs, which have high potential for translation to humans. The highly studied hERG R56Q variant has an uncertain mechanism of arrhythmogenicity despite being associated with

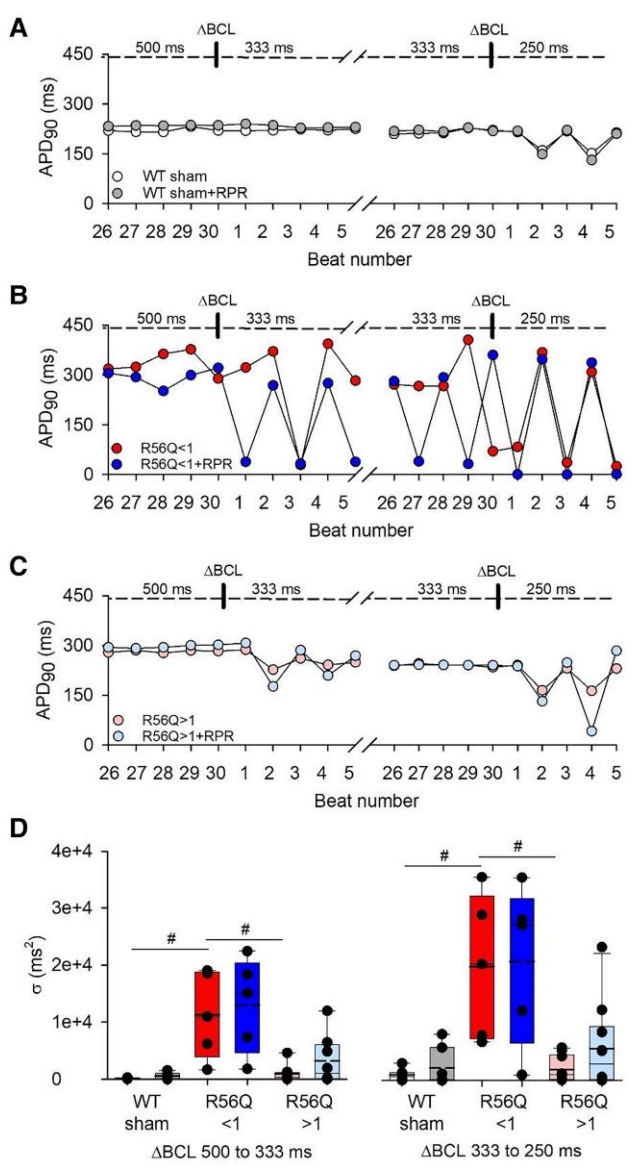

Figure 6 APD_{90} adaptation to abrupt rate transitions. (*A–C*) Diary plots of measured APD_{90} values from an example WT sham cell (*A*), hERG R56Q cell with an ERP/APD_{90} ratio <1 (*B*), and hERG R56Q cell with an ERP/APD_{90} ratio >1 (*C*) in the absence and presence of 10 μM RPR260243. APD_{90} values are plotted during rate transitions from a BCL of 500 to 333 ms (left) and from 333 to 250 ms (right). In each case, the APD_{90} from the final five beats at the longer BCL and the initial five beats at the new BCL are shown. (*D*) Box plot representations of the variance of the APD_{90} of the first five beats following BCL transition from 500 to 333 ms (left) and from 333 to 250 ms (right). Each dot represents data from a single cell. WT sham ($n = 7$), WT sham with 10 μM RPR260243 ($n = 7$, WT sham + RPR), hERG R56Q with an ERP/APD_{90} ratio <1 ($n = 5$, R56Q < 1), hERG R56Q with an ERP/APD_{90} ratio <1 with 10 μM RPR260243 ($n = 5$, R56Q < 1 + RPR), hERG R56Q with an ERP/APD_{90} ratio >1 ($n = 10$, R56Q > 1), hERG R56Q with an ERP/APD_{90} ratio >1 with 10 μM RPR260243 ($n = 10$, R56Q > 1 + RPR). #Significant difference (In all box plots, each dot represents data from a single cell). #Significantly different mean value (two-way repeated measures ANOVA with Holm–Sidak *post hoc* test; $P \leq 0.05$).

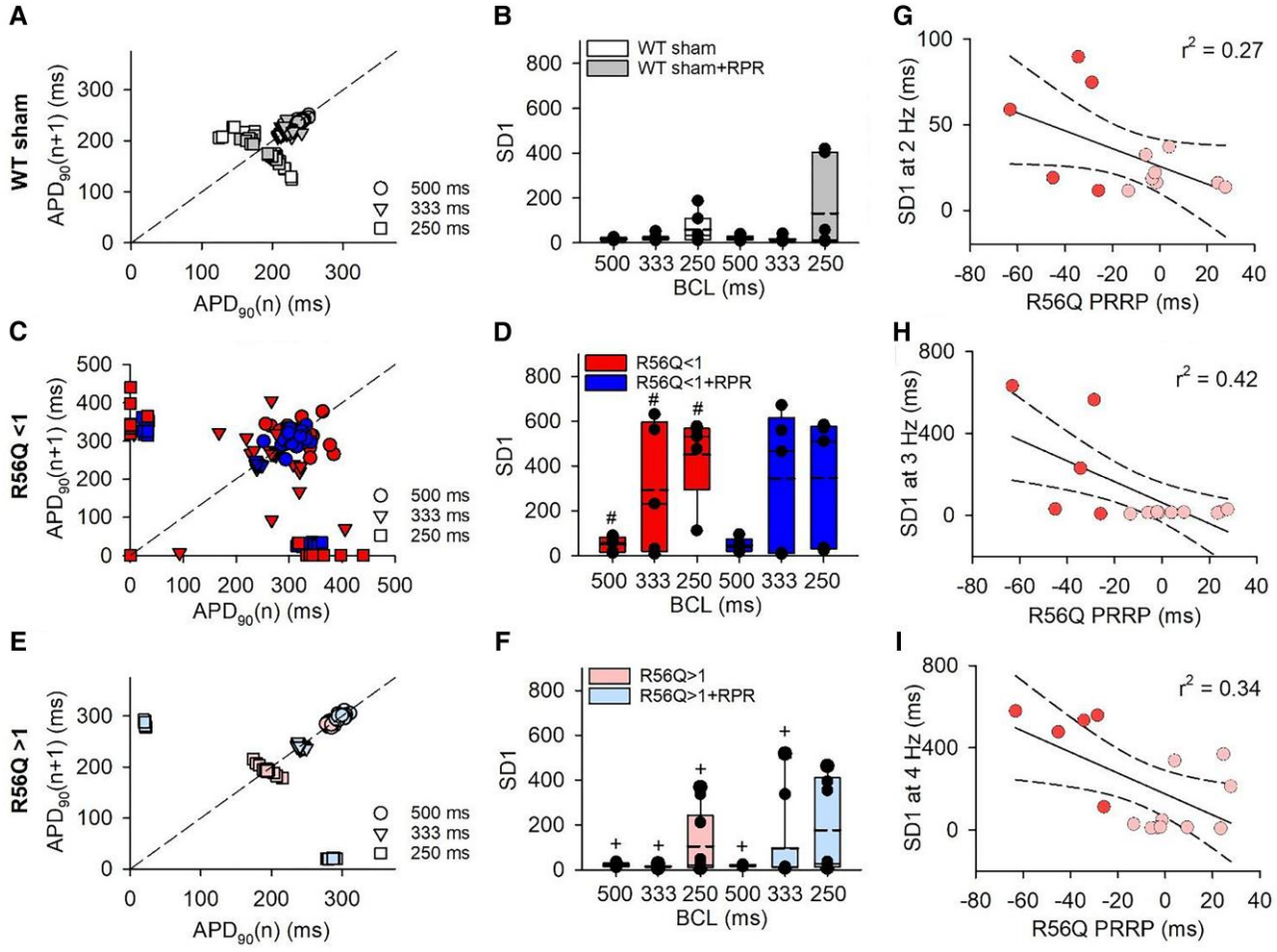

Figure 7 Beat-to-beat variability of APD_{90} in hiPSC-CMs during constant pacing. (*A*, *C*, and *E*) Poincare plots of the *n*th APD_{90} during the *n*th action potential plotted against that during the (*n* + 1) action potential during 20 steady-state beats at a range of BCLs in an example WT sham cell (*A*), a hERG R56Q cell with an ERP/APD90 ratio <1 (R56Q < 1; *C*), and a hERG R56Q cell with an ERP/APD90 ratio >1 (R56Q > 1; *E*). Data are shown in the absence and presence of 10 μM RPR260243. (*B*, *D*, and *F*) Box plot representations of short-term variability, SD1, values calculated from ellipses constrained by the data with 95% confidence drawn for each individual cell (not shown) at each BCL in each cell. Each dot represents the SD1 value of a single cell. #Significant difference from WT sham (in all box plots, each dot represents data from a single cell). #Significantly different mean value, +Significant difference from R56Q < 1 (two-way repeated measures ANOVA with Holm–Sidak *post hoc* test; $P \leq 0.05$). (*G*, *H*, and *I*) Linear regression plots describing the relationship between PRRP and SD1 variance at 2, 3, and 4 Hz across all hERG R56Q variant cells. Solid lines represent regression fits and dashed lines reflect 95% confidence intervals. r^2 values were 0.27 ($P = 0.0045$), 0.42 ($P = 0.009$), and 0.34 ($P = 0.022$) for the SD1 variance at 2, 3, and 4 Hz, respectively.

LQTS2. We show that, without significant effect on mean APD_{90}, the hERG R56Q variant: (i) introduces marked beat-to-beat variability in APD during constant cycle length pacing; (ii) enhances variance of APD during rate transitions; and (iii) results in more variable membrane responses to premature stimulations. These findings indicate that the hERG R56Q variant induces pathogenicity by facilitating heterogeneous APD dynamics within individual cells that could provide the substrate for the spatial dispersion of repolarization underlying arrhythmic events. In addition, we found that application of the Type 1 hERG channel activator, RPR260243, reduces the APD variance, increases the post-repolarization refractoriness and increases the protection against action potential firing in response to premature stimulation in hERG R56Q hiPSC-CMs. These findings illustrate the potential protection afforded by hERG activator compounds that slow channel deactivation against both triggered activity and electrical heterogeneity, which occurs without significant APD_{90} shortening and the associated risk of early repolarization.

4.1 An hiPSC-CM model to test the consequences of targeted manipulation of hERG channel deactivation gating

Study of the hERG R56Q variant and the effects of application of RPR260243 enabled assessment of the pathogenic consequences of accelerated deactivation and targeted pharmacological rescue of slow deactivation in hiPSC-CMs and their implications on indices of arrhythmogenicity. Dofetilide-sensitive I_{Kr} recordings from hERG R56Q hiPSC-CMs showed the fast-deactivating channel phenotype and subsequent slowing of deactivation following application of RPR260243. Accelerated deactivation gating is the most pronounced characteristic of the R56Q variant,[18] although recent evidence suggests that the membrane stability of channel protein might be affected by the variant, resulting in a modest (~20%) reduction in surface expression,[23] which is supported by a possible trend towards reduced expression observed in *Figure 1D*. At the concentration used in the current study (10 μM), the effect of RPR260243 is reasonably specific to

Table 4 Poincare SD1 values of beat-to-beat APD_{90} variability

SD1 values at BCL (ms)	WT sham	WT sham + RPR	hERG R56Q ERP/ $APD_{90} < 1$	hERG R56Q ERP/ $APD_{90} < 1$ + RPR	hERG R56Q ERP/ $APD_{90} > 1$	hERG R56Q ERP/ $APD_{90} > 1$ + RPR
500	17.1 ± 2.8	19.6 ± 4.7	50.8 ± 15.3[a]	45.1 ± 14.1	20.9 ± 3.2[b]	18.7 ± 1.5[b]
333	21.2 ± 5.7	15.9 ± 4.5	293.3 ± 130.7[a]	343.5 ± 140.2	15.0 ± 1.8[b]	95.8 ± 57.0[b]
250	59.0 ± 24.9	131.6 ± 72.8	451.7 ± 86.5[a]	345.1 ± 129.4	105.0 ± 45.7[b]	176.9 ± 66.2

[a]Significantly different from WT sham.
[b]Significantly different from hERG R56Q ERP/$APD_{90} < 1$.

hERG channel deactivation, although higher concentrations reduce hERG inactivation,[14] and the effects of RPR260243 on hERG channels are reported to be specific, with little effect on other cardiac ion channels.[19] Thus, this study not only provides the first demonstration of the phenotypic effects of the hERG R56Q variant and of the RPR260243 activator in hiPSC-CMs but also enables functional testing of targeted manipulation of hERG deactivation gating.

4.2 Steady-state action potential responses

Previous studies have reported or predicted differing effects of the R56Q variant on the APD with some observations of APD prolongation[24] and others showing no effect.[14] This has made understanding the pathogenic mechanism challenging, despite extensive study of this variant. We observed no overall effect of the R56Q variant on the mean APD_{90} in hiPSC-CMs. However, the significantly greater variance in the APD_{90} indicates underlying heterogeneity in these cells that was not present in other measurements such as MDP and action potential amplitude, and we propose that this contributes to arrhythmia predisposition in hERG R56Q variant carriers. We also observed no significant effect of RPR260243 on steady-state action potential properties. While a hERG channel activator may be expected to shorten the APD, this observation in hiPSC-CMs is consistent with previous reports that RPR260243 had little effect on the APD in *ex vivo* guinea pig hearts.[19] However, we found that the variability in APD_{90} in hERG R56Q cells was reduced by the application of RPR260243. These findings suggest that the functional impacts of manipulating hERG channel deactivation are not immediately apparent as changes in the mean steady-state APD_{90}.

4.3 Electrical restitution properties in hiPSC-CMs

The ERC is a well-studied relationship between APD and the preceding DI that has been used to predict the inducibility of ventricular arrhythmias.[25] In particular, the steepness of the restitution curve has been used to predict ventricular tachycardia (VT)/VF vulnerability, and drugs that reduce the slope of the relationship prevent VT/VF.[25,26] To the best of our knowledge, the ERCs describing APD restitution dynamics in the present study are the first reports in single hiPSC-CMs. The restitution behaviour that we observed in WT sham hiPSC-CMs was similar to that reported from *in vivo* and *in vitro* studies[27] with rate-dependent shortening of the APD that was best described by a sigmoidal relationship. The maximum slope of the electrical restitution relationship was found to be protocol dependent, with standard ERC slopes being shallower than dynamic ERC slopes. This is consistent with previous studies[28,29] and highlights the influence of preceding activity that influences membrane refractoriness, which is described as cellular 'memory.'[30] Interestingly, the maximal slopes of both SERC (~3.0) and DERC (~2.0) observed in the present study are steeper than many previous reports in humans (~0.2–1.2).[27] Since a steeper relationship has been associated with increased VF incidence,[26] our findings may indicate that relatively immature isolated hiPSC-CMs may be more susceptible to arrhythmia, although there are also reports that the maximal slope may not be a good predictor of lethality.[31] The maximum slope of the ERCs recorded from hERG R56Q hiPSC-CMs were not significantly different from those recorded in WT sham cells, and application of RPR260243 also had no significant effect in either cell line. We hypothesized that APs would be triggered at shorter DIs in hERG R56Q cells, consistent with reduced protection against premature beats. Comparing the ERCs in *Figure 3A* and *C* shows that this is indeed the case. For example, at a DI of close to 0 ms the WT sham produces only a short pseudo-AP, while in the hERG R56Q, an AP of ~150 ms in duration is triggered. In other words, the ERC is left shifted in hERG R56Q compared with WT sham. This is consistent with the prolonged APD_{90} of the ECVR that we observed in hERG R56Q, as well as the more negative PRRP that we observed in some R56Q cells. These findings suggest that the arrhythmogenicity associated with the hERG R56Q variant does not arise from an altered ability of the APD to shorten at faster rates, but instead relates to increased membrane responses at short DIs.

4.4 Facilitated excitability and encroachment

We found that application of RPR260243 significantly prolonged the PRRP in both WT sham and hERG R56Q cells. This is consistent with our working hypothesis that slowed hERG channel deactivation increases hERG protective currents in response to premature stimulation, which resist facilitated excitation and reduce encroachment. This is also consistent with previous reports of RPR260243-induced prolongation of the PRRP in zebrafish hearts.[13] As an indicator of the balance between the refractory period and the APD, antiarrhythmic drugs that prolong the PRRP are associated with improved outcomes.[21,32] Previously, two other hERG channel activators, NS-1643 and MC-II-157c, have been reported or predicted to prolong the PRRP in *ex vivo* guinea pig hearts[11] or *in silico* cellular and tissue models.[33,34] In these cases, however, the PRRP prolongation was associated with activator-induced shortening of the APD, which resulted overall in a decreased refractory period that was predicted to slow the propagating wave front.[33,34] Such dispersion of repolarization would sustain triggered activity, i.e. increase the tissue substrate, leading to re-entrant arrhythmia.[35] Moreover, simulations suggested that NS-1643 and MC-II-157c also increased the spatiotemporal vulnerable window where wave-front conduction might be slowed.[33,34] Thus, the APD shortening action of these hERG activators may predispose an arrhythmogenic substrate. Similarly, excessive APD shortening produced by activators, such as ICA-105574 and LUF7244 have been suggested to risk overcorrection and enhanced, rather than reduced, arrhythmogenicity.[10,36,37] In the present study, the action of the Type 1 activator, RPR260243, which preferentially targets deactivation gating, prolongs the PRRP without significantly shortening the APD and consequently does not increase the refractory period or risk early repolarization. In the light of this, we propose that the effects of RPR260243 may reduce the substrate for re-entry and therefore offer antiarrhythmic potential. Testing in multicellular preparations and/or *in silico* models to measure wave-front propagation and the vulnerable window are needed to further investigate this possibility.

Another effect of RPR260243 was to rescue aberrant behaviour of the ECVR in hERG R56Q cells. We found that the ECVRs to premature stimulation in hERG R56Q cells had a slower rise time and were longer in duration than those in WT sham cells. Moreover, the earliest captured responses were significantly more variable in hERG R56Q than those

observed in WT sham cells. While there was no correlation between these ECVR measures and the PRRP or ERP/APD_{90} ratio in hERG R56Q cells, these observations indicate that the R56Q variant both slows, and increases the heterogeneity of, ventricular responses to premature stimulations. The former would be expected to increase conduction time, which would shorten the excitation wavelength and facilitate re-entry. The latter would be expected to result in temporal and spatial ventricular heterogeneity that would in turn facilitate propagation of triggered activity.[34] We found that RPR260243 restored WT-like rise time and duration of the earliest captured response and significantly reduced the variability of these measures in hERG R56Q cells. Thus, in addition to prolonging the PRRP, these findings further indicate effective antiarrhythmic promise for the RPR260243 hERG activator.

4.5 Beat-to-beat variability during constant pacing and rate-transition variance

hERG R56Q cells showed marked heterogeneity in beat-to-beat APD_{90} and the response to abrupt rate changes. While the APD_{90} in hERG R56Q cells with a positive PRRP and higher ERP/APD_{90} ratio was quite stable, hERG R56Q cells with a negative PRRP and low ERP/APD_{90} ratio showed high dispersion of APD_{90}. This was observed, both during pacing at constant cycle length as an increased beat-to-beat variability in Poincare plots and as increased variance in APD_{90} response to rate transitions. Indeed, negative PRRP values in R56Q hERG cells were significantly correlated with high beat-to-beat variance, long APD_{90}, and a high triangulation index. These findings indicate heterogeneous and irregular APD dynamics in the hERG R56Q variant leading to electrical instability. In addition to improved responses to premature stimulation during abrupt changes in cycle length, RPR260243 application reduced the APD_{90} dispersion during pacing at constant cycle length and converted unstable rate-transition responses to a more stable 2:1 capture, which reduced heterogeneity in hERG R56Q cells.

4.6 A proposed mechanism for hERG R56Q-induced arrhythmogenicity and the antiarrhythmic action of the RPR260243 hERG activator

Taken together, the data lead us to propose plausible mechanisms by which the hERG R56Q variant may both facilitate triggered activity and establish a pathogenic substrate, and by which RPR260243 may afford protection. We observed marked heterogeneity in the phenotype of hERG R56Q variant cells with some cells (those with a low ERP/APD_{90} ratio) exhibiting decreased resistance to premature stimulations, high beat-to-beat APD_{90} variability/dispersion during pacing at constant cycle length with prolonged APD_{90} and increased triangulation, and unstable APD_{90} responses to rate transitions, while other hERG R56Q variant cells (those with a high ERP/APD_{90} ratio) had increased refractoriness that may contribute to conduction block. Such irregular dispersion of the APD_{90} would lead to temporal and spatial heterogeneity of repolarization[25] that may predispose re-entrant arrhythmia[38] and has been shown in *in silico* studies to lead to spiral wave break into multiple wavelets[39] that facilitate VF. Spatial dispersion of repolarization due to the heterogeneous APD may also facilitate propagation of triggered activity within the tissue by increasing the vulnerable window.[34] The presence of different cellular phenotypes in the hERG R56Q variant would be expected to further promote cellular electrical heterogeneity. For example, reduced protection against premature excitation in cells with a low ERP/APD_{90} ratio may trigger activation wave fronts that meet slowed conduction regions due to the relative refractoriness of neighbouring tissue, i.e. cells with a high ERP/APD_{90} ratio, and this would to facilitate re-entry. The heterogeneity in rise time and duration of ventricular responses to premature activity that we observed in the hERG R56Q cell population would also be expected to contribute. The hERG R56Q variant may therefore predispose re-entrant excitation as a result of an aberrant premature depolarization that arrives during constant cycle length activity, which already has an intrinsically higher APD_{90} variance, or during abrupt cycle length transitions, such as in response to a startle, a known trigger for LQTS2-related events.[40] This enhanced risk of triggered activity, coupled with a facilitated substrate for re-entry created by the marked cellular electrical heterogeneity might lead to sustained arrhythmia.[41] This may occur in addition to a mild reduction in stability of the membrane protein[23] that would be expected to further enhance the arrhythmogenic potential of the R56Q variant. In this manner, while the steady-state APD_{90} in the hERG R56Q variant is not significantly different from that in WT, presenting as an unremarkable QTc in the electrocardiogram of an individual carrier similar to that observed in concealed LQTS,[42] there remains an intrinsic elevated underlying arrhythmia risk.[43]

The underlying cause of the heterogeneous phenotypic manifestation of the hERG R56Q variant warrants further investigation. Perhaps variable expression levels of hERG1a and hERG1b[44] in different cells influence the effect of the R56Q variant on I_{Kr} in individual cells. CRISPR–Cas9 editing the H70R hERG1a variant into hiPSC-CMs was recently associated with an altered ratio of hERG1a to hERG1b protein expression.[45] We found no significant changes in the relative membrane expression of hERG1a and hERG1b protein between WT sham and hERG R56Q cell lysates. While this suggests no effect of the variant in broad terms, these data do not report the relative expression in each individual cell. Another possibility is that there is variable compensation from other ion currents that is dependent on relative channel expression in different cells. For example, the balance of I_{Kr} with other ion currents, such as I_{Ca}, is known to influence the impact of I_{Kr} modification on APD_{90} and its variance,[46] and this may be a factor that varies on a cell-to-cell basis. The lack of observed correlation between the PRRP and the MDP in R56Q cells suggests that altered sodium channel availability may not be responsible for the variance in phenotype in these cells. We hypothesize that cells with a low ERP/APD_{90} ratio may be more susceptible to encroachment due to reduced protection, while cells with a high ERP/APD_{90} ratio may be more resilient to this effect. Interestingly, a previous study using patient-derived LQTS3 iPSC-CMs discovered variability in the APD phenotype in different hiPSC-CM cell types.[47] In a subsequent *in silico* study, Paci *et al.*[48] established that the repolarization reserve served as a key determinant of the heterogenous APD, which is in turn determined by differences in ionic current expression in hiPSC-CMs. Further studies of relative ion channel expression in individual cells and/or experiments in multicellular preparations or *in silico* may further understanding on the underlying substrate.

RPR260243 enhances the post-repolarization refractory period and decreases the heterogeneity of excitability in the hERG R56Q variant, resulting in reduced ectopic activity and more stable rate transitions during abrupt cycle length changes. By prolonging the PRRP without the proarrhythmogenic risk of shortening the APD_{90} often observed with hERG activators, RPR260243 may offer safer protective action. Thus, targeting hERG channel deactivation may be an attractive mechanism to afford protection in variants that cause accelerated deactivation gating, or in pharmacologically rescued trafficking-deficient variants that exhibit fast deactivation. Studies that improve understanding of the molecular mechanism of action of RPR260243,[49] combined with those that evaluate the potential for RPR260243-induced rescue of different variants, and the effects of variant location and mechanism of dysfunction will be of significant benefit.

5. Limitations

There are several limitations to these studies to be considered. First, our experiments were performed on functionally immature cardiomyocytes with ion channel expression that differs from that of adult cardiomyocytes.[50] In particular, the low expression or lack of I_{K1} in immature hiPSC-CMs[50] results in a relatively depolarized diastolic membrane potential and subsequent pre-inactivation of I_{Na}. This, combined with the slow recovery kinetics of I_{to},[51] may affect refractory and restitution characteristics.[52] However, our hERG R56Q cells had a reasonably hyperpolarized

maximum diastolic depolarization that was similar to our WT sham cells, and therefore, this is unlikely to explain the differences that we observed in the variant, or the effects of RPR260243. Secondly, despite the study being suitably powered to detect a 20% difference in APD_{90} (that may be considered clinically relevant) between WT sham and hERG R56Q cells during steady-state pacing with 95% confidence, the relatively low sample size of our study means that we cannot rule out the possibility that there is a small, but significant difference of uncertain clinical relevance in the mean APD_{90} between the WT and R56Q. Lastly, differentiation of hiPSC-CMs produces a heterogeneous population of cardiomyocytes.[53] To mitigate some of this heterogeneity, we used standardized kit-based approaches, and our study of single cells allowed us to select specifically for ventricular cells. This approach produced APD characteristics with relatively low variability in WT sham cells even during complex stimulation paradigms, which demonstrate low differentiation-induced cell-to-cell heterogeneity. Further studies, for example with a multi-electrode array, optical mapping, or sharp electrodes to explore and test our findings in electrically coupled multicellular monolayer or three-dimensional cardioid preparations will be valuable future directions.

Supplementary material

Supplementary material is available at *Cardiovascular Research* online.

Acknowledgements

The authors acknowledge the kind gift of the pCCC vector from Dr Francis Lynn, Dr Alvin Shrier, and Dr Leon Glass for insightful discussions, and Dr Tom Bury for designing a restitution simulation programme.

Conflict of interest: None declared.

Funding

This research was conducted using grant support from the Canadian Institutes of Health Research (grant no. 156168 held by T.W.C.) and the Natural Sciences and Engineering Research Council of Canada (grant no. RG-PIN-2020-04429 held by T.W.C.). D.V.H. was supported by the Michael Smith Foundation for Health Research BC Trainee Program.

Data availability

The data underlying this article are available in the article and in its online supplementary material.

References

1. Sanguinetti MC, Jiang C, Curran ME, Keating MT. A mechanistic link between an inherited and an acquired cardiac arrhythmia: HERG encodes the I_{Kr} potassium channel. *Cell* 1995;**81**:299–307.
2. Curran ME, Splawski I, Timothy KW, Vincen GM, Green ED, Keating MT. A molecular basis for cardiac arrhythmia: HERG mutations cause long QT syndrome. *Cell* 1995;**80**:795–803.
3. Moss AJ, Schwartz PJ, Crampton RS. The long QT syndrome. Prospective longitudinal study of 328 families. *Circulation* 1991;**84**(3):1136–1144.
4. Crotti L, Celano G, Dagradi F, Schwartz PJ. Congenital long QT syndrome. *Orphanet J Rare Dis* 2008;**3**:18.
5. Barsheshet A, Dotsenko O, Goldenberg I. Genotype-specific risk stratification and management of patients with long QT syndrome. *Ann Noninvasive Electrocardiol* 2013;**18**:499–509.
6. Priori SG, Napolitano C, Schwartz PJ. Low penetrance in the long-QT syndrome. *Circulation* 1999;**99**:529–533.
7. Goldenberg I, Horr S, Moss AJ, Lopes CM, Barsheshet A, McNitt S, Zareba W, Andrews ML, Robinson JL, Locati EH, Ackerman MJ, Benhorin J, Kaufman ES, Napolitano C, Platonov PG, Priori SG, Qi M, Schwartz PJ, Shimizu W, Towbin JA, Vincent GM, Wilde AAM, Zhang L. Risk for life-threatening cardiac events in patients with genotype-confirmed long-QT syndrome and normal-range corrected QT intervals. *J Am Coll Cardiol* 2011;**57**:51–59.
8. Wilde AAM, Amin AS, Postema PG. Diagnosis, management and therapeutic strategies for congenital long QT syndrome. *Heart* 2022;**108**:332–338.
9. Sala L, Yu Z, Ward-van Oostwaard D, van Veldhoven JPD, Moretti A, Laugwitz K-L, Mummery CL, IJzerman AP, Bellin M. A new hERG allosteric modulator rescues genetic and drug-induced long-QT syndrome phenotypes in cardiomyocytes from isogenic pairs of patient induced pluripotent stem cells. *EMBO Mol Med* 2016;**8**:1065–1081.
10. Perry MD, Ng C-A, Mangala MM, Ng TYM, Hines AD, Liang W, Xu MJO, Hill AP, Vandenberg JI. Pharmacological activation of I_{Kr} in models of long QT type 2 risks overcorrection of repolarization. *Cardiovasc Res* 2020;**116**:1434–1445.
11. Hansen RS, Olesen S-P, Rønn LCB, Grunnet M. In vivo effects of the I_{Kr} agonist NS3623 on cardiac electrophysiology of the guinea pig. *J Cardiovasc Pharmacol* 2008;**52**:35–41.
12. O'Hare BJ, John Kim CS, Hamrick SK, Ye D, Tester DJ, Ackerman MJ. Promise and potential peril with lumacaftor for the trafficking defective type 2 long-QT syndrome-causative variants, p.G604S, p.N633S, and p.R685P, using patient-specific re-engineered cardiomyocytes. *Circulation* 2020;**13**:466–475.
13. Shi YP, Pang Z, Venkateshappa R, Gunawan M, Kemp J, Truong E, Chang C, Lin E, Shafaattalab S, Faizi S, Rayani K, Tibbits GF, Claydon VE, Claydon TW. The hERG channel activator, RPR260243, enhances protective I_{Kr} current early in the refractory period reducing arrhythmogenicity in zebrafish hearts. *Am J Physiol Heart Circ Physiol* 2020;**319**:H251–H261.
14. Kemp JM, Whittaker DG, Venkateshappa R, Pang Z, Johal R, Sergeev V, Tibbits GF, Mirams GR, Claydon TW. Electrophysiological characterization of the hERG R56Q LQTS variant and targeted rescue by the activator RPR260243. *J Gen Physiol* 2021;**153**:e202112923.
15. Concordet J-P, Haeussler M. CRISPOR: intuitive guide selection for CRISPR/Cas9 genome editing experiments and screens. *Nucleic Acids Res* 2018;**46**:W242–W245.
16. Churko JM, Garg P, Treutlein B, Venkatasubramanian M, Wu H, Lee J, Wessells QN, ChenS-Y, Chen W-Y, Chetal K, Mantalas G, Neff N, Jabart E, Sharma A, Nolan GP, Salomonis N, Wu JC. Defining human cardiac transcription factor hierarchies using integrated single-cell heterogeneity analysis. *Nat Commun* 2018;**9**:4906.
17. Horváth A, Lemoine MD, Löser A, Mannhardt I, Flenner F, Uzun AU, Neuber C, Breckwoldt K, Hansen A, Girdauskas E, Reichenspurner H, Willems S, Jost N, Wettwer E, Eschenhagen T, Christ T. Low resting membrane potential and low inward rectifier potassium currents are not inherent features of hiPSC-derived cardiomyocytes. *Stem Cell Reports* 2018;**10**:822–833.
18. Chen J, Zou A, Splawski I, Keating MT, Sanguinetti MC. Long QT syndrome-associated mutations in the Per-Arnt-Sim (PAS) domain of HERG potassium channels accelerate channel deactivation. *J Biol Chem* 1999;**274**:10113–10118.
19. Kang J, Chen X-L, Wang H, Ji J, Cheng H, Incardona J, Reynolds W, Viviani F, Tabart M, Rampe D. Discovery of a small molecule activator of the human ether-a-go-go-related gene (HERG) cardiac K+ channel. *Mol Pharmacol* 2005;**67**:827–836.
20. Koller BS, Karasik PE, Solomon AJ, Franz MR. Relation between repolarization and refractoriness during programmed electrical stimulation in the human right ventricle. *Circulation* 1995;**91**:2378–2384.
21. Kirchhof P, Degen H, Franz MR, Eckardt L, Fabritz L, Milberg P, Läer S, Neumann J, Breithardt G, Haverkamp W. Amiodarone-induced postrepolarization refractoriness suppresses induction of ventricular fibrillation. *J Pharmacol Exp Ther* 2003;**305**:257–263.
22. Selvaraj RJ, Picton P, Nanthakumar K, Chauhan VS. Steeper restitution slopes across right ventricular endocardium in patients with cardiomyopathy at high risk of ventricular arrhythmias. *Am J Physiol Heart Circ Physiol* 2007;**292**:H1262–H1268.
23. Foo B, Barbier C, Guo K, Vasantharuban J, Lukacs GL, Shrier A. Mutation-specific peripheral and ER quality control of hERG channel cell-surface expression. *Sci Rep* 2019;**9**:6066.
24. Liu Q, Trudeau MC, Matthew C. Eag domains regulate LQT mutant hERG channels in human induced pluripotent stem cell-derived cardiomyocytes. *PLoS One* 2015;**10**:e0123951.
25. Koller ML, Riccio ML, Gilmour RF Jr. Dynamic restitution of action potential duration during electrical alternans and ventricular fibrillation. *Am J Physiol Heart Circ Physiol* 1998;**275**:H1635–H1642.
26. Garfinkel A, Kim Y-H, Voroshilovsky O, Qu Z, Kil JR, Lee M-H, Karagueuzian HS, Weiss JN, Chen P-S. Preventing ventricular fibrillation by flattening cardiac restitution. *Proc Natl Acad Sci U S A* 2000;**97**:6061–6066.
27. Taggart P, Lab M. Cardiac mechano-electric feedback and electrical restitution in humans. *Prog Biophys Mol Biol* 2008;**97**:452–460.
28. Goldhaber JI, Xie L-H, Duong T, Motter C, Khuu K, Weiss JN. Action potential duration restitution and alternans in rabbit ventricular myocytes. *Circ Res* 2005;**96**:459–466.
29. Koller ML, Maier SKG, Gelzer AR, Bauer WR, Meesmann M, Gilmour RF. Altered dynamics of action potential restitution and alternans in humans with structural heart disease. *Circulation* 2005;**112**:1542–1548.
30. Gilmour RF, Otani NF, Watanabe MA. Memory and complex dynamics in cardiac Purkinje fibers. *Am J Physiol Heart Circ Physiol* 1997;**272**:H1826–H1832.
31. Narayan SM, Franz MR, Lalani G, Kim J, Sastry A. T-wave alternans, restitution of human action potential duration, and outcome. *J Am Coll Cardiol* 2007;**50**:2385–2392.
32. Franz MR, Gray RA, Karasik P, Moore HJ, Singh SN. Drug-induced post-repolarization refractoriness as an antiarrhythmic principle and its underlying mechanism. *Europace* 2014;**16**:iv39–iv45.
33. Peitersen T, Grunnet M, Benson AP, Holden AV, Holstein-Rathlou N-H, Olesen S-P. Computational analysis of the effects of the hERG channel opener NS1643 in a human ventricular cell model. *Heart Rhythm* 2008;**5**:734–741.
34. Colman MA, Perez Alday EA, Holden AV, Benson AP. Trigger vs. substrate: multi-dimensional modulation of QT-prolongation associated arrhythmic dynamics by a hERG channel activator. *Front Physiol* 2017;**8**:757.
35. Pandit SV, Jalife J. Rotors and the dynamics of cardiac fibrillation. *Circ Res* 2013;**112**:849–862.
36. Meng J, Shi C, Li L, Du Y, Xu Y. Compound ICA-105574 prevents arrhythmias induced by cardiac delayed repolarization. *Eur J Pharmacol* 2013;**718**:87–97.
37. Qiu B, Wang Y, Li C, Guo H, Xu Y. Utility of the JT peak interval and the JT area in determining the proarrhythmic potential of QT-shortening agents. *J Cardiovasc Pharmacol Ther* 2019;**24**:160–171.

38. Coronel R, Wilms-Schopman FJG, Opthof T, Janse MJ. Dispersion of repolarization and arrhythmogenesis. *Heart Rhythm* 2009;**6**:537–543.
39. Karma A. Electrical alternans and spiral wave breakup in cardiac tissue. *Chaos* 1994;**4**: 461–472.
40. Cox KO, Wang BX. Long QT syndrome type 2: mechanism-based therapies. *Future Cardiol* 2021;**17**:1453–1463.
41. Antzelevitch C. Heterogeneity and cardiac arrhythmias: an overview. *Heart Rhythm* 2007;**4**: 964–972.
42. Schwartz PJ, Crotti L, Insolia R. Long QT syndrome: from genetics to management. *Circ Arrhythm Electrophysiol* 2012;**5**:868–877.
43. Priori SG, Schwartz PJ, Napolitano C, Bloise R, Ronchetti E, Grillo M, Vicentini A, Spazzolini C, Nastoli J, Bottelli G, Folli R, Cappelletti D. Risk stratification in the long-QT syndrome. *N Engl J Med* 2003;**348**:1866–1874.
44. Otsuji TG, Minami I, Kurose Y, Yamauchi K, Tada M, Nakatsuji N. Progressive maturation in contracting cardiomyocytes derived from human embryonic stem cells: qualitative effects on electrophysiological responses to drugs. *Stem Cell Res* 2010;**4**:201–213.
45. Feng L, Zhang J, Lee CH, Kim G, Liu F, Petersen AJ, Lim E, Anderson CL, Orland KM, Robertson GA, Eckhardt LL, January CT, Kamp TJ. Long QT syndrome KCNH2 variant induces hERG1a/1b subunit imbalance in patient-specific induced pluripotent stem cell–derived cardiomyocytes. *Circ Arrhythm Electrophysiol* 2021;**14**(4):e009343.
46. Ballouz S, Mangala MM, Perry MD, Heitmann S, Gillis JA, Hill AP, Vandenberg JI. Co-expression of calcium and hERG potassium channels reduces the incidence of proarrhythmic events. *Cardiovasc Res* 2021;**117**:2216–2227.
47. Ma D, Wei H, Zhao Y, Lu J, Li G, Sahib NBE, Tan TH, Wong KY, Shim W, Wong P, Cook SA, Liew R. Modeling type 3 long QT syndrome with cardiomyocytes derived from patient-specific induced pluripotent stem cells. *Int J Cardiol* 2013;**168**:5277–5286.
48. Paci M, Passini E, Severi S, Hyttinen J, Rodriguez B. Phenotypic variability in LQT3 human induced pluripotent stem cell-derived cardiomyocytes and their response to antiarrhythmic pharmacologic therapy: an in silico approach. *Heart Rhythm* 2017;**14**:1704–1712.
49. Zangerl-Plessl E-M, Wu W, Sanguinetti MC, Stary-Weinzinger A. Binding of RPR260243 at the intracellular side of the hERG1 channel pore domain slows closure of the helix bundle crossing gate. *Front Mol Biosci* 2023;**10**:1137368.
50. Doss MX, Di Diego JM, Goodrow RJ, Wu Y, Cordeiro JM, Nesterenko VV, Barajas-Martínez H, Hu D, Urrutia J, Desai M, Treat JA, Sachinidis A, Antzelevitch C. Maximum diastolic potential of human induced pluripotent stem cell-derived cardiomyocytes depends critically on I_{Kr}. *PLoS One* 2012;**7**:e40288.
51. Cordeiro JM, Nesterenko VV, Sicouri S, Goodrow RJ, Treat JA, Desai M, Wu Y, Doss MX, Antzelevitch C, Di Diego JM. Identification and characterization of a transient outward K+ current in human induced pluripotent stem cell-derived cardiomyocytes. *J Mol Cell Cardiol* 2013;**60**:36–46.
52. Decker KF, Heijman J, Silva JR, Hund TJ, Rudy Y. Properties and ionic mechanisms of action potential adaptation, restitution, and accommodation in canine epicardium. *Am J Physiol Heart Circ Physiol* 2009;**296**:H1017–H1026.
53. Ma J, Guo L, Fiene SJ, Anson BD, Thomson JA, Kamp TJ, Kolaja KL, Swanson BJ, January CT. High purity human-induced pluripotent stem cell-derived cardiomyocytes: electrophysiological properties of action potentials and ionic currents. *Am J Physiol Heart Circ Physiol* 2011;**301**:H2006–H2017.

Translational perspective

Inherited long QT syndrome is a cardiac repolarization disorder that predisposes cardiac arrhythmias. Evaluation of the pathogenicity of individual genetic variants can be challenging to determine, especially when the QTc is borderline or normal. Using a hERG channel variant that is associated with sudden death, but that does not appreciably delay repolarization, we identify a novel mechanism for variant-induced electrical instability and arrhythmia. We also show that a targeted hERG activator molecule reduces arrhythmia risk without over-correction and the associated risk of early repolarization. Our studies highlight the potential for improved risk stratification and targeted enhancement of hERG variant function.